

Analytical characterization of gaseous slip flow and heat transport through a parallel-plate microchannel with a centered porous substrate

Keyong Wang

*School of Mechanical Engineering,
Shanghai University of Engineering Science, Shanghai, China*

Kambiz Vafai

*Department of Mechanical Engineering,
University of California Riverside, Riverside, California, USA, and*

Dazhong Wang

*School of Mechanical Engineering,
Shanghai University of Engineering Science, Shanghai, China*

Abstract

Purpose – The purpose of this paper is to analytically perform gaseous slip flow and heat transfer analysis within a parallel-plate microchannel partially filled with a centered porous medium under local thermal non-equilibrium (LTNE) condition. Heat transfer of gaseous flow in a porous microchannel is analytically studied. Energy communication at the porous-fluid interface is considered by two approaches: the gas rarefaction negatively impacts the heat transfer performance, and the optimum ratio of porous thickness is found to be around 0.8.

Design/methodology/approach – Both Models A and B are utilized to consider the heat flux splitting for the fluid and solid phases at the porous-fluid interface.

Findings – Analytical solutions for the fluid and solid phase temperature distributions and the Nusselt number are derived. In the no-slip flow limit, the present analytical solutions are validated by the partially and fully filled cases available in the literature.

Research limitations/implications – The continuum flow (no-slip flow) is only a special case of the slip flow. Meanwhile, the effects of pertinent parameters on the heat transfer are also discussed.

Practical implications – A survey of available literature mentioned above indicates a shortage of information for slip flow and heat transfer in partially filled porous systems. The main objective of the present study is to investigate the slip flow and heat transfer characteristics for forced convection through a microchannel partially filled with a porous medium under LTNE condition. The porous substrate is placed at the center of the microchannel. Analytical solutions for the temperature distributions of the fluid and solid phases and the Nusselt number at the microchannel wall are obtained.

Originality/value – Heat transfer of gaseous flow in a porous microchannel is analytically studied. Energy communication at the porous-fluid interface is considered by two approaches: the gas rarefaction negatively impacts the heat transfer performance, and the optimum ratio of porous thickness is found to be around 0.8. Gaseous slip flow and heat transfer analysis is analytically performed within a parallel-plate microchannel partially filled with a centered porous medium under LTNE condition. Analytical solutions for the fluid and solid phase temperature distributions and the



Conflict of interest: none declared.

This work was supported by the Visiting Scholar Program for Young Faculty in Shanghai, China. The authors would like to acknowledge this support.

Nusselt number are derived for the first time. The effects of pertinent parameters on the heat transfer are also discussed. Compared with the results obtained for the continuum flow regime, the gas rarefaction negatively impacts the heat transfer efficiency and has little influence on the optimal porous thickness.

Keywords Microchannel, Porous medium, Local thermal non-equilibrium, Rarefaction effect

Paper type Research paper

Nomenclature

a_{sf}	interfacial area per unit volume of the porous medium (m^{-1})	<i>Greek symbols</i>	
Bi	Biot number, $h_{sf} a_{sf} H^2 / k_{s,eff}$	α	velocity slip coefficient, $[(2-\sigma_v)/\sigma_v]Kn$
c_p	specific heat of the fluid ($\text{J kg}^{-1} \text{K}^{-1}$)	β	temperature jump coefficient, $[(2-\sigma_t)/\sigma_t][2\varphi/(\varphi+1)]Kn/Pr$
Da	Darcy number	γ	ratio of the heat flux at the interface to that at the channel wall
D_h	hydraulic diameter of the microchannel, $4H$ (m)	δ	$= \sqrt{Bi(1+\kappa)/\kappa}$
f	Fanning friction factor	ε	porosity
h_{sf}	interstitial heat transfer coefficient ($\text{W m}^{-2} \text{K}^{-1}$)	η	dimensionless transverse coordinate, y/H
H	half-height of the microchannel (m)	θ	dimensionless temperature, $k_{s,eff}(T-T_w)/(q_w H)$
k_f	thermal conductivity of the fluid ($\text{W m}^{-1} \text{K}^{-1}$)	k	ratio of the effective thermal conductivity of the fluid to that of the solid, $k_{f,eff}/k_{s,eff}$
$k_{f,eff}$	effective thermal conductivity of the fluid ($\text{W m}^{-1} \text{K}^{-1}$)	λ	molecular mean free path (m)
k_s	thermal conductivity of the solid ($\text{W m}^{-1} \text{K}^{-1}$)	ξ	ratio of porous medium thickness to the channel half-height
$k_{s,eff}$	effective thermal conductivity of the solid ($\text{W m}^{-1} \text{K}^{-1}$)	μ	dynamic viscosity of the fluid (Pas)
K	permeability (m^2)	ρ	density of the fluid (kg/m^3)
Kn	Knudsen number	σ_t	thermal accommodation coefficient
M	ratio of the effective viscosity of the porous medium to the viscosity of the clear fluid	σ_v	tangential momentum accommodation coefficient
Nu	Nusselt number at the channel wall	ω	porous media shape factor, $\sqrt{1/DaM}$
p	pressure (Pa)	<i>Subscripts/superscripts</i>	
P	dimensionless pressure gradient	<i>eff</i>	effective
Pr	Prandtl number	<i>f</i>	fluid
q_w	imposed heat flux on the wall (W/m^2)	<i>f1</i>	fluid in the clear region
Re	Reynolds number	<i>f2</i>	fluid in the porous region
T	temperature (K)	<i>i</i>	porous-fluid interface
u	fluid velocity (m/s)	<i>in</i>	inlet
\hat{u}	dimensionless velocity	<i>m</i>	mean value
x	longitudinal coordinate (m)	<i>s</i>	solid
y	transverse coordinate (m)	<i>w</i>	channel wall subject to a constant heat flux

1. Introduction

Porous medium filling is a potential way to enhance the heat transfer ability of thermal systems (Pavel and Mohamad, 2004; Zehforoosh and Hossainpour, 2010; Satyamurty and Bhargavi, 2010; Qu *et al.*, 2012; Nimvari *et al.*, 2012; Lasiello *et al.*, 2015). A great deal of

research has been carried out to study the filling configurations such as partial porous filling and full porous filling. Compared with the fully filled system, the partially filled one is considered as a promising configuration due to its relatively low pressure loss and high heat transfer (Xu *et al.*, 2011). On the other hand, there are two primary models, namely local thermal equilibrium (LTE) (Chen *et al.*, 2015; Yuan *et al.*, 2015) and local thermal non-equilibrium (LTNE) (Yang and Vafai, 2010, 2011a), which can be utilized for representing the heat transport through a porous medium. When the temperature difference between the fluid and solid phases is substantial, the LTE model would break down, but the LTNE model can capture this temperature difference using two different energy equations for two individual phases (Yang and Vafai, 2010, 2011a) which significantly reflects on the level of heat transfer (Nimvari *et al.*, 2012; Yang *et al.*, 2012; Wang *et al.*, 2015c).

In a composite system with partial porous insertion, there usually exist two distinct regions, i.e. the porous region and the clear region without porous matrix, where the behavior of fluid flow and heat transfer exhibits different characteristics (Yang and Vafai, 2011a; Shokouhmand *et al.*, 2011; Yang *et al.*, 2012; Mahdavi *et al.*, 2014). Although the superiority of LTNE to LTE is applicable to more general analysis for partially filled porous structures, an extra complexity would be encountered in the modeling of involved porous-fluid interface at which the physical mechanism of splitting the heat flux between the fluid and solid phases is still open and the determination of the interfacial thermal boundary conditions remains a scientific challenge (Yang and Vafai, 2011a, b; Vafai and Yang, 2013; Mahmoudi *et al.*, 2014). However, a basic consensus is that the heat flux transmits from the clear fluid to the two phases within the porous medium at the porous-fluid interface in two distinct ways which were later known as Models A and B (Vafai and Kim, 1990; Amiri *et al.*, 1995; Yang and Vafai, 2011b; Vafai and Yang, 2013). The first one assumes that the heat flux is split between the fluid and solid phases within the porous medium based on their effective conductivities and associated temperature gradients while the second one assumes that each of individual phases at the interface receives an equal amount of heat flux from the clear fluid.

Mohamad (2003) studied numerically a tube partially or fully occupied by porous media. It was found that in the configuration of partial filling, the heat transfer rate was increased while the pressure drop was decreased in comparison with that of full filling. Yang and Vafai (2011a) investigated analytically the heat flux bifurcation within a channel partially filled with a porous medium under LTNE condition. In their study, the range of validity for all three interface Models A, B and C was established. Yang *et al.* (2012) analytically assessed the two cases of partial porous medium filling. It was revealed that in a comparatively low range of pumping power the heat transfer performance in a tube with a porous medium core is higher than that of the tube with a wall covered with a porous medium layer whereas in a high range of pumping power the latter is superior to the former. Mahmoudi and Maerefat (2011) analytically investigated the forced convection flow in a channel partially filled with a porous medium. They concluded that the optimal porous thickness ratio is 0.8 for enhancement of heat transfer at a reasonable expense of pressure drop. Subsequently, Mahmoudi *et al.* (2014) carried out a comprehensive analysis of the two interface Models A and B. They also discussed the validity of LTE assumption. Torabi *et al.* (2015) carried out an analytical study on the heat transfer and entropy generation in a parallel-plate channel partially filled with a porous medium. The lower wall of the channel was exposed to a constant heat flux and the upper wall was assumed in the adiabatic condition. Bifurcation phenomena for both heat transfer and entropy generation were observed.

In the past decades, the progress in micro fabrication technology has led to the miniaturization of various fluidic systems such as heat exchangers, pumps, actuators, etc. At the micro scale, the wall effect on the fluid flow and heat transfer would become considerable. This effect associated with gaseous flow through micropassages where the molecular mean free path (λ) of the flowing gas is comparable to the characteristic dimension of fluid domain, is called the rarefaction effect. The degree of rarefaction of the gas and the validity of continuum flow assumption are determined by the Knudsen number (Kn), depending on which four flow regimes exist: $Kn \leq 10^{-3}$ for the continuum flow regime, $10^{-3} < Kn \leq 10^{-1}$ for the slip flow regime, $10^{-1} < Kn \leq 10$ for the transition flow regime and $Kn > 10$ for the free molecular flow regime. Here, the Knudsen number is defined as the ratio of the molecular mean free path to the characteristic dimension. Although the continuum model does not hold for the slip flow regime where molecular collisions with the walls dominate over intermolecular collisions, the gaseous flow can still be analyzed by the conventional Navier-Stokes and energy equations with modifications of boundary conditions at the walls (Renksizbulut *et al.*, 2006; Haddad *et al.*, 2007; Hooman, 2009). One of the earliest contributions to the gaseous flow and heat transfer in a fully filled porous microchannel under the LTNE condition was analytically conducted by Buonomo *et al.* (2014) who derived the temperature distributions and the Nusselt number for Model A. Mahmoudi (2015) analytically studied the effect of internal heat generation on the forced convective heat transfer in a microchannel fully filled with a porous medium saturated with rarefied gas. Wang *et al.* (2015a) performed an analytical investigation related to gaseous flow and heat transfer in an annulus fully filled with a porous medium. They pointed out that the configuration of constant heat flux at the inner wall and adiabatic outer wall creates more heat transfer enhancement within the porous medium as compared to that of constant heat flux at the outer wall and adiabatic inner wall. In a separate work, Wang *et al.* (2015d) analytically considered the effect of gas rarefaction on a circular tube fully filled with a porous medium.

A survey of available literature mentioned above indicates a shortage of information for slip flow and heat transfer in partially filled porous systems. The main objective of the present study is to investigate the slip flow and heat transfer characteristics for forced convection through a microchannel partially filled with a porous medium under LTNE condition. The porous substrate is placed at the center of the microchannel. Analytical solutions for the temperature distributions of the fluid and solid phases and the Nusselt number at the microchannel wall are obtained. Both Models A and B are employed for incorporating the heat flux splitting between the fluid and solid phases within the porous medium at the porous-fluid interface. The effects of pertinent parameters such as effective thermal conductivity ratio, Biot number, Knudsen number, Darcy number and porous medium thickness are also discussed.

2. Mathematical modeling

2.1 Governing equations

The schematic diagram of the problem under consideration is illustrated in Figure 1. The fluid flows through a parallel-plate microchannel partially filled with a centered porous medium without phase change. The microchannel walls are assumed impermeable and uniformly heated by a constant heat flux q_w . Due to the symmetry of

the thermal system, only one half is analyzed. Meanwhile, the following assumptions are invoked in the current study:

- the flow is assumed to be incompressible due to the fact that in most practical situations the Mach number (Ma) for a flow in a porous medium will be small compared with unity (Nield and Kuznetsov, 2007);
- the steady-state hydrodynamically and thermally fully developed conditions are desired with temperature independent properties;
- natural convection, dispersion and radiative heat transfer are negligible;
- the LTNE between the fluid and solid phases in the porous region is allowed; and
- longitudinal conduction of the fluid in both porous and clear regions is negligible for high Peclet number (Pe) (Narasimhan *et al.*, 2001).

The momentum equation in the clear region reads:

$$\mu \frac{d^2 u_{f1}}{dy^2} - \frac{dp}{dx} = 0 \tag{1}$$

The Brinkman-extended Darcy momentum equation is employed in the porous region:

$$\mu_{eff} \frac{d^2 u_{f2}}{dy^2} - \frac{\mu}{K} u_{f2} - \frac{dp}{dx} = 0 \tag{2}$$

The energy equation for the fluid in the clear region gives:

$$k_f \frac{\partial^2 T_{f1}}{\partial y^2} = \rho c_p u_{f1} \frac{\partial T_{f1}}{\partial x} \tag{3}$$

The energy equation for the fluid phase in the porous region reads:

$$k_{f,eff} \frac{\partial^2 T_{f2}}{\partial y^2} + h_{sf} a_{sf} (T_s - T_{f2}) = \rho c_p u_{f2} \frac{\partial T_{f2}}{\partial x} \tag{4}$$

The energy equation for the solid phase in the porous region is expressed as:

$$k_{s,eff} \frac{\partial^2 T_s}{\partial y^2} - h_{sf} a_{sf} (T_s - T_{f2}) = 0 \tag{5}$$

where u is the fluid velocity, μ the dynamic viscosity of the fluid, k_f and k_s the thermal conductivities of the fluid and solid phases, $k_{f,eff}$ and $k_{s,eff}$ the effective thermal

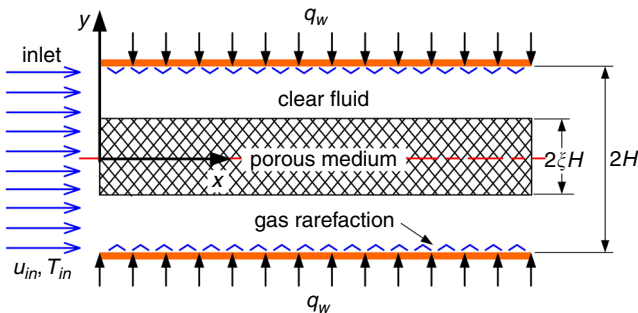


Figure 1.
Schematic diagram of a parallel-plate microchannel partially filled with a centered porous medium

conductivities of the fluid and solid phases, and $k_{f,eff} = \epsilon k_f$, $k_{s,eff} = (1-\epsilon)k_s$, μ_{eff} the effective viscosity, K the permeability of the porous medium, p the applied pressure and T_f , T_s , ϵ , ρ and c_p the fluid and solid temperatures, the porosity, the density and specific heat of the fluid, h_{sf} and a_{sf} are, respectively, the heat transfer coefficient and the specific surface area which couples the two energy equations for the fluid and solid phases in the porous region.

2.2 Boundary conditions

The symmetry conditions at $y = 0$ are:

$$\left. \frac{du_{f2}}{dy} \right|_{y=0} = 0 \tag{6}$$

$$\left. \frac{\partial T_{f2}}{\partial y} \right|_{y=0} = \left. \frac{\partial T_s}{\partial y} \right|_{y=0} = 0 \tag{7}$$

Beyond the continuum limit, the fluid particles adjacent to the wall surface no longer reach the velocity of the surface due to the presence of rarefaction phenomenon at the micro scale. More importantly, the velocity slip and relaxed fluid-solid contact of surfaces may lead to the temperature jump. At the microchannel wall ($y = H$), hence, the following first-order velocity slip and temperature jump conditions at the walls need to be utilized (Karniadakis *et al.*, 2005):

$$u_{slip} = u_{f1} \Big|_{y=H} = -\alpha H \left. \frac{du_{f1}}{dy} \right|_{y=H}, \quad \alpha = \frac{2-\sigma_v}{\sigma_v} \text{Kn} \tag{8}$$

$$T_{jump} = T_{f1} \Big|_{y=H} - T_w = -\beta H \left. \frac{\partial T_{f1}}{\partial y} \right|_{y=H}, \quad \beta = \frac{2-\sigma_t}{\sigma_t} \frac{2\varphi}{\varphi+1} \frac{\text{Kn}}{\text{Pr}} \tag{9}$$

Additionally, the total heat flux transmitted from the heated wall to the clear fluid can be expressed as:

$$k_f \left. \frac{\partial T_{f1}}{\partial y} \right|_{y=H} = q_w \tag{10}$$

where T_w is the temperature of the microchannel wall, φ the specific heat ratio, Pr the Prandtl number, σ_v and σ_t are, respectively, the tangential momentum and thermal accommodation coefficients, both of which are dependent on the surface finish, the fluid temperature and pressure. As highlighted by Cai *et al.* (2007) and Bahrami *et al.* (2012), the values of σ_v and σ_t should be less than unity based on the experimental results (Bahrami *et al.*, 2012). In the current study, $\sigma_v = \sigma_t = 0.85$, $\gamma = 1.4$ and $Pr = 0.707$ are employed unless otherwise noted. It should be noted that $\text{Kn} = \lambda/H$ and obviously the velocity slip and temperature jump given by Equations (8) and (9) increase as λ increases.

At the porous-fluid interface ($y = \xi H$), the fluid velocity should be specified as (Mahmoudi *et al.*, 2014; Mahmoudi, 2015):

$$\mu \left. \frac{du_{f1}}{dy} \right|_{y=\xi H^+} = \mu_{eff} \left. \frac{du_{f2}}{dy} \right|_{y=\xi H^-} \tag{11}$$

$$u_{f1}|_{y=\xi H^+} = u_{f2}|_{y=\xi H^-} \tag{12}$$

Based on the work of Amiri *et al.* (1995) and Yang and Vafai (2010, 2011a), the thermal boundary conditions for Model A are given by:

$$k_f \frac{\partial T_{f1}}{\partial y} \Big|_{y=\xi H^+} = k_{f,eff} \frac{\partial T_{f2}}{\partial y} \Big|_{y=\xi H^-} + k_{s,eff} \frac{\partial T_s}{\partial y} \Big|_{y=\xi H^-} = q_i \tag{13}$$

$$T_{f1}|_{y=\xi H^+} = T_{f2}|_{y=\xi H^-} = T_s|_{y=\xi H^-} = T_i \tag{14}$$

whereas the thermal boundary conditions for Model B are casted as (Yang and Vafai, 2010, 2011a):

$$k_f \frac{\partial T_{f1}}{\partial y} \Big|_{y=\xi H^+} = k_{f,eff} \frac{\partial T_{f2}}{\partial y} \Big|_{y=\xi H^-} = k_{s,eff} \frac{\partial T_s}{\partial y} \Big|_{y=\xi H^-} = q_i \tag{15}$$

$$T_{f1}|_{y=\xi H^+} = T_{f2}|_{y=\xi H^-} \tag{16}$$

where q_i and T_i are the total heat flux and the temperature at the porous-fluid interface.

In the partial filling microchannel, the bulk mean flow velocity is defined by (Mahmoudi *et al.*, 2014; Mahmoudi, 2015):

$$u_m = \frac{1}{H} \left(\int_0^{\xi H^-} u_{f2} dy + \int_{\xi H^+}^H u_{f1} dy \right) \tag{17}$$

Integrating Equation (3) from the interface to the channel wall and incorporating the boundary conditions given by Equations (10) and (13) produces:

$$\rho c_p \frac{\partial T_{f1}}{\partial x} \int_{\xi H^+}^H u_{f1} dy = q_w - q_i \tag{18}$$

Adding Equations (4) and (5), integrating the resultant equation from the center to the interface and applying the boundary conditions given by Equation (13) leads to:

$$\rho c_p \frac{\partial T_{f2}}{\partial x} \int_0^{\xi H^-} u_{f2} dy = q_i \tag{19}$$

In a fully developed flow, it should be noted that $\partial T_{f1}/\partial x = \partial T_{f2}/\partial x = \partial T_f/\partial x = \text{const}$. Adding Equations (18) and (19) and considering Equation (17) yields:

$$\rho c_p \frac{\partial T_f}{\partial x} \Big|_{Model A} = \frac{q_w}{H u_m} \tag{20}$$

Combining Equations (20) and (19) results in Model A-based heat flux prediction at the porous-fluid interface as:

$$\gamma|_{Model A} = \frac{q_i}{q_w} \Big|_{Model A} = \frac{1}{H u_m} \int_0^{\xi H^-} u_{f2} dy \tag{21}$$

Following the similar way as done for Model A, adding Equations (4) and (5), integrating the resultant equation from the center to the interface and applying the boundary condition given by Equation (15) yields:

Gaseous slip
flow and heat
transport

$$\rho c_p \frac{\partial T_{f2}}{\partial x} \int_0^{\xi H^-} u_{f2} dy = 2q_i \quad (22)$$

The physical mechanism for Equation (22) has been explained by Amiri *et al.* (1995), Lee and Vafai (1999), Yang and Vafai (2010, 2011a) and Mahmoudi *et al.* (2014), and then, Equations (18) and (22) are added to obtain the following relation:

$$\rho c_p \frac{\partial T_f}{\partial x} \Big|_{Model B} = \frac{q_w + q_i}{Hu_m} \quad (23)$$

Combining Equations (23) and (22) leads to Model B-based heat flux prediction at the interface as:

$$\gamma \Big|_{Model B} = \frac{q_i}{q_w} \Big|_{Model B} = \frac{\int_0^{\xi H^-} u_{f2} dy}{2Hu_m - \int_0^{\xi H^-} u_{f2} dy} \quad (24)$$

2.3 Hydrodynamic analysis

The non-dimensionalization procedure is of primary significance in the hydrodynamic and thermal analysis (Glicksman, 1988; de Souza Mendes, 2007). This procedure can remarkably reduce the amount of variables involved in the governing equations, which is helpful for gaining insight into the essence of fluid flow and heat transfer. After introducing the following the dimensionless variables:

$$\eta = \frac{y}{H}, \quad \hat{u} = \frac{u}{u_m}, \quad P = \frac{K dp}{\mu u dz}, \quad Da = \frac{K}{H^2}, \quad \omega = \sqrt{\frac{1}{DaM}}, \quad M = \frac{\mu_{eff}}{\mu} \quad (25)$$

the momentum Equations (1) and (2) and associated boundary conditions given by Equations (6), (8), (11) and (12) can be written in the dimensionless forms:

$$\frac{d^2 \hat{u}_{f1}}{d\eta^2} - \frac{P}{Da} = 0 \quad (26)$$

$$M \frac{d^2 \hat{u}_{f2}}{d\eta^2} - \frac{1}{Da} (\hat{u}_{f2} + P) = 0 \quad (27)$$

$$\frac{d\hat{u}_{f2}}{d\eta} \Big|_{\eta=0} = 0 \quad (28)$$

$$\frac{d\hat{u}_{f1}}{d\eta} \Big|_{\eta=\xi^+} = M \frac{d\hat{u}_{f2}}{d\eta} \Big|_{\eta=\xi^-} \quad (29)$$

$$\hat{u}_{f1}|_{\eta=\xi^+} = \hat{u}_{f2}|_{\eta=\xi^-} \quad (30)$$

$$\hat{u}_{f1}|_{\eta=1} = -\alpha \frac{d\hat{u}_{f1}}{d\eta} \Big|_{\eta=1} \quad (31)$$

862

Thus, the velocity distributions in the porous and clear regions can be simultaneously evaluated by solving Equations (26) and (27) subject to the boundary conditions given by Equations (28)-(31) as:

$$\hat{u}_{f1} = A_1 + A_2\eta + \frac{1}{2} \frac{P}{Da} \eta^2 \quad (32)$$

$$\hat{u}_{f2} = A_3 \cosh(\omega\eta) - P \quad (33)$$

where the constants A_1, A_2, A_3 and P are presented in the Appendix. Upon obtaining the velocity fields in the porous and clear regions, we can proceed with the pressure drop information in terms of the Fanning friction factor f and the Reynolds number Re :

$$fRe = -\frac{8P}{Da} \quad (34)$$

where $f = -(4H)(dp/dz)/(\rho u_m^2)$ and $Re = \rho u_m(2H)/\mu$.

Attention will now be turned to the heat flux ratio γ at the porous-fluid interface. Using Equation (25), the heat flux ratio for Models A and B given by Equations (21) and (24) can be explicitly evaluated in the following dimensionless forms:

$$\gamma|_{Model A} = \int_0^{\xi^-} \hat{u}_{f2} d\eta = \frac{A_3}{\omega} \sinh(\omega\xi) - P\xi \quad (35)$$

$$\gamma|_{Model B} = \frac{\int_0^{\xi^-} \hat{u}_{f2} d\eta}{2 - \int_0^{\xi^-} \hat{u}_{f2} d\eta} = \frac{A_3 \sinh(\omega\xi) - P\omega\xi}{2\omega - A_3 \sinh(\omega\xi) - P\omega\xi} \quad (36)$$

2.4 Heat transfer analysis

2.4.1 Model A-based temperature prediction. To normalize the energy equations and associated boundary conditions, the following dimensionless variables are utilized as:

$$\kappa = \frac{k_{f,eff}}{k_{s,eff}}, \quad Bi = \frac{h_{sf} a_{sf} H^2}{k_{s,eff}}, \quad \theta_f = \frac{k_{s,eff}(T_f - T_w)}{q_w H}, \quad \theta_s = \frac{k_{s,eff}(T_s - T_w)}{q_w H} \quad (37)$$

where κ is the ratio of the effective thermal conductivity of the fluid to that of the solid and Bi is the equivalent Biot number for the inserted porous substrate.

Upon substituting Equation (37) into Equations (3)-(5) and (7), (9), (10), (13) and (14) and considering Equations (32) and (33), we obtain the dimensionless energy equations and boundary conditions as follows.

For the fluid in the clear region:

$$\frac{\kappa}{\varepsilon} \frac{\partial^2 \theta_{f1}}{\partial \eta^2} = A_1 + A_2\eta + \frac{1}{2} \frac{P}{Da} \eta^2 \quad (38)$$

For the fluid phase in the porous region:

$$\kappa \frac{\partial^2 \theta_{f2}}{\partial \eta^2} + \text{Bi}(\theta_s - \theta_{f2}) = A_3 \cosh(\omega \eta) - P \quad (39)$$

For the solid phase in the porous region:

$$\frac{\partial^2 \theta_s}{\partial \eta^2} - \text{Bi}(\theta_s - \theta_{f2}) = 0 \quad (40)$$

For the thermal boundary conditions:

$$\left. \frac{\partial \theta_{f2}}{\partial \eta} \right|_{\eta=0} = \left. \frac{\partial \theta_s}{\partial \eta} \right|_{\eta=0} = 0 \quad (41)$$

$$\theta_{f1} \Big|_{\eta=\xi^+} = \theta_{f2} \Big|_{\eta=\xi^-} = \theta_s \Big|_{\eta=\xi^-} \quad (42)$$

$$\theta_{f1} \Big|_{\eta=1} = -\beta \left. \frac{\partial \theta_{f1}}{\partial \eta} \right|_{\eta=1}, \quad \left. \frac{\partial \theta_{f1}}{\partial \eta} \right|_{\eta=1} = \frac{\varepsilon}{\kappa} \quad (43)$$

The ordinary differential Equation (38) is integrated twice and the temperature distribution of the flow in the clear region is obtained as:

$$\theta_{f1} = B_1 + B_2 \eta + \frac{\varepsilon}{6\kappa} \left(3A_1 \eta^2 + A_2 \eta^3 + \frac{P}{4\text{Da}} \eta^4 \right) \quad (44)$$

It should be noted that Equations (39) and (40) are coupled. Hence, decoupling techniques are required for the solutions of fluid and solid temperatures in the porous region. As categorized by Wang *et al.* (2015b), these techniques involve the direct decoupling method (DDM) and the indirect decoupling method (IDM). Additional higher order boundary conditions must be established in DDM whereas only original boundary conditions are required in IDM. In the current study, therefore, IDM is employed as the solution procedure due to its easy-to-use analytic characteristics. By adding the two dimensionless energy Equations (39) and (40), we can obtain the following equation for a new variable $\kappa \theta_{f2} + \theta_s$:

$$\frac{\partial^2}{\partial \eta^2} (\kappa \theta_{f2} + \theta_s) = A_3 \cosh(\omega \xi) - P \quad (45)$$

Combining Equations (41) and (45) and solving for $\kappa \theta_{f2} + \theta_s$, we obtain the solid phase temperature distribution as follows:

$$\theta_s = B_3 + \frac{A_3}{\omega^2} \cosh(\omega \eta) - \frac{P}{2} \eta^2 - \kappa \theta_{f2} \quad (46)$$

Substituting Equation (46) into Equation (39) and considering Equation (33) results in:

$$\frac{\partial^2 \theta_{f2}}{\partial \eta^2} - \delta^2 \theta_{f2} = \frac{A_3}{\kappa} \left(1 - \frac{\text{Bi}}{\omega^2} \right) \cosh(\omega \eta) + \frac{\text{Bi}}{\kappa} \left(\frac{P}{2} \eta^2 - B_3 \right) - \frac{P}{\kappa} \quad (47)$$

where $\delta = \sqrt{\text{Bi}(1 + \kappa)/\kappa}$. Thus, the fluid phase temperature distribution can be readily obtained by solving the ordinary differential Equation (47) together with the boundary condition given by Equation (41) as:

$$\theta_{f2} = B_4 \cosh(\delta \eta) + \frac{A_3}{\kappa} \left(1 - \frac{\text{Bi}}{\omega^2} \right) \frac{\cosh(\omega \eta)}{\omega^2 - \delta^2} + \frac{1}{1 + \kappa} \left[P \left(\frac{1}{\kappa \delta^2} \frac{\eta^2}{2} \right) + B_3 \right] \quad (48)$$

where the constants B_1, B_2, B_3 and B_4 involved in Equations (44), (46) and (48) are presented in the Appendix. To this end, the two energy Equations (39) and (40) are decoupled. As addressed by Mahjoob and Vafai (2009a, b), Yang and Vafai (2010, 2011a) and Wang *et al.* (2015a, c, d), the LTE solutions can be obtained with the temperature of fluid and solid phases in the porous medium being assumed to be equal. Following this way, the temperature distribution in the porous region is readily obtained as:

$$\theta_{f2} = \theta_s = \frac{1}{1 + \kappa} \left[B'_3 + \frac{A_3}{\omega^2} \cosh(\omega \eta) - \frac{P}{2} \eta^2 \right] \quad (49)$$

where the constant B'_3 is presented in the Appendix.

2.4.2 Model B-based temperature prediction. For this approach, each of the two phases at the interface is exposed to a heat flux q_i . The dimensionless energy equations and the associated boundary conditions can be obtained by substituting Equation (37) into Equations (3)-(5), (7), (9), (15) and (16) and considering Equations (32) and (33). Hence, the energy equation for the fluid in the clear region is found to be:

$$\frac{\kappa}{\varepsilon} \frac{\partial^2 \theta_{f1}}{\partial \eta^2} = (1 + \gamma) \left[A_1 + A_2 \eta + \frac{1}{2} \frac{P}{\text{Da}} \eta^2 \right] \quad (50)$$

Fluid phase energy equation in the porous region is:

$$\kappa \frac{\partial^2 \theta_{f2}}{\partial \eta^2} + \text{Bi}(\theta_s - \theta_{f2}) = (1 + \gamma) [A_3 \cosh(\omega \zeta) - P] \quad (51)$$

and the solid phase energy equation in the porous region is given by:

$$\frac{\partial^2 \theta_s}{\partial \eta^2} - \text{Bi}(\theta_s - \theta_{f2}) = 0 \quad (52)$$

The associated energy boundary conditions are:

$$\left. \frac{\partial \theta_{f2}}{\partial \eta} \right|_{\eta=0} = \left. \frac{\partial \theta_s}{\partial \eta} \right|_{\eta=0} = 0 \quad (53)$$

$$\theta_{f1}|_{\eta=\xi^+} = \theta_{f2}|_{\eta=\xi^-}, \quad \frac{\partial \theta_s}{\partial \eta}|_{\eta=\xi^-} = \frac{\gamma}{\kappa} \quad (54)$$

$$\theta_{f1}|_{\eta=1} = -\beta \frac{\partial \theta_{f1}}{\partial \eta}|_{\eta=1}, \quad \frac{\partial \theta_{f1}}{\partial \eta}|_{\eta=1} = \frac{\varepsilon}{\kappa} \quad (55)$$

The temperature distribution of the fluid in the clear region is obtained by integrating the ordinary differential Equation (50) twice as:

$$\theta_{f1} = C_1 + C_2 \eta + \frac{\varepsilon(1+\gamma)}{6\kappa} \left(3A_1 \eta^2 + A_2 \eta^3 + \frac{P}{4Da} \eta^4 \right) \quad (56)$$

Using the DDM employed for Model A, the two dimensionless energy Equations (51) and (52) for Model B are added to yield the following ordinary differential equation for a new variable $\kappa \theta_{f2} + \theta_s$:

$$\frac{\partial^2}{\partial \eta^2} (\kappa \theta_{f2} + \theta_s) = (1+\gamma) [A_3 \cosh(\omega \xi) - P] \quad (57)$$

Combining Equations (53) and (57) and solving for $\kappa \theta_{f2} + \theta_s$, we obtain the solid phase temperature distribution as follows:

$$\theta_s = C_3 + (1+\gamma) \left[\frac{A_3}{\omega^2} \cosh(\omega \eta) - \frac{P}{2} \eta^2 \right] - \kappa \theta_{f2} \quad (58)$$

Substituting Equation (58) into Equation (51) and incorporating Equation (33) results in:

$$\frac{\partial^2 \theta_{f2}}{\partial \eta^2} - \delta^2 \theta_{f2} = \frac{A_3}{\kappa} (1+\gamma) \left(1 - \frac{\text{Bi}}{\omega^2} \right) \cosh(\omega \eta) + \frac{\text{Bi}}{\kappa} \left[\frac{P}{2} (1+\gamma) \eta^2 - C_3 \right] - \frac{P}{\kappa} (1+\gamma) \quad (59)$$

After considering the boundary condition given by Equation (53), the fluid phase temperature distribution can be achieved by solving Equation (59) as:

$$\theta_{f2} = C_4 \cosh(\delta \eta) + \frac{A_3}{\kappa} (1+\gamma) \left(1 - \frac{\text{Bi}}{\omega^2} \right) \frac{\cosh(\omega \eta)}{\omega^2 - \delta^2} + \frac{1}{1+\kappa} \left[P(1+\gamma) \left(\frac{1}{\kappa \delta^2} - \frac{\eta^2}{2} \right) + C_3 \right] \quad (60)$$

where the constants C_1 , C_2 , C_3 and C_4 involved in Equations (56), (58) and (60) are presented in the Appendix.

2.5 Heat transfer correlations

From the analytical solutions for the velocity and temperature distributions, the Nusselt number on the microchannel walls with the constant heat flux, being the primary parameter of interest in heat transfer analysis, is determined based on the thermal conductivity of the gas. The wall heat transfer coefficient is obtained from:

866

$$h_w = \frac{q_w}{T_w - T_{f,b}} \tag{61}$$

thus the Nusselt number from:

$$Nu = \frac{D_h h_w}{k_f} = -\frac{4\varepsilon}{\kappa \theta_{f,b}} \tag{62}$$

for the partial filling case ($\xi < 1$) and:

$$Nu = \frac{D_h h_w}{k_{f,eff}} = -\frac{4}{\kappa \theta_{f,b}} \tag{63}$$

for the fully filled case ($\xi \rightarrow 1$). Here D_h is the hydraulic diameter of the microchannel and $\theta_{f,b}$ the dimensionless bulk mean fluid temperature defined by:

$$\theta_{f,b} = \int_0^{\xi^-} \hat{u}_{f2} \theta_{f2} d\eta + \int_{\xi^+}^1 \hat{u}_{f1} \theta_{f1} d\eta \tag{64}$$

which can be explicitly expressed as:

$$\begin{aligned} \theta_{f,b}|_{Model A} = & \frac{A_3 B_4}{\omega^2 - \delta^2} [\omega \cosh(\delta \xi) \sinh(\omega \xi) - \delta \cosh(\omega \xi) \sinh(\delta \xi)] \\ & + \frac{1}{4\kappa\omega} \frac{A_3^2}{\omega^2 - \delta^2} \left(1 - \frac{Bi}{\omega^2}\right) [2\omega \xi + \sinh(2\omega \xi)] \\ & - \frac{A_3 P}{2(1+\kappa)} \frac{1}{\omega^3} [(2 + \omega^2 \xi^2) \sinh(\omega \xi) - 2\omega \xi \cosh(\omega \xi)] \\ & + \frac{A_3}{\omega} \left[\frac{1}{1+\kappa} \left(\frac{P}{\kappa \delta^2} + B_3\right) - \frac{P}{\kappa} \left(1 - \frac{Bi}{\omega^2}\right) \frac{1}{\omega^2 - \delta^2} \right] \sinh(\omega \xi) \\ & - B_4 \frac{P}{\delta} \sinh(\delta \xi) + \frac{P^2}{6(1+\kappa)} \xi^3 - \frac{P}{1+\kappa} \left(\frac{P}{\kappa \delta^2} + B_3\right) \xi \\ & + A_1 B_1 (1 - \xi) + \frac{1}{2} (A_1 B_2 + A_2 B_1) (1 - \xi^2) \\ & + \frac{1}{6} \left(\frac{\varepsilon}{\kappa} A_1^2 + 2A_2 B_2 + \frac{B_1 P}{Da}\right) (1 - \xi^3) + \frac{1}{2} \left(\frac{\varepsilon}{3\kappa} A_1 A_2 + \frac{B_2 P}{4Da}\right) (1 - \xi^4) \\ & + \frac{1}{30} \frac{\varepsilon}{\kappa} \left(\frac{7P}{4Da} A_1 + A_2^2\right) (1 - \xi^5) \\ & + \frac{1}{48} \frac{\varepsilon P}{\kappa Da} A_2 (1 - \xi^6) + \frac{1}{336} \frac{\varepsilon}{\kappa} \left(\frac{P}{Da}\right)^2 (1 - \xi^7) \end{aligned} \tag{65}$$

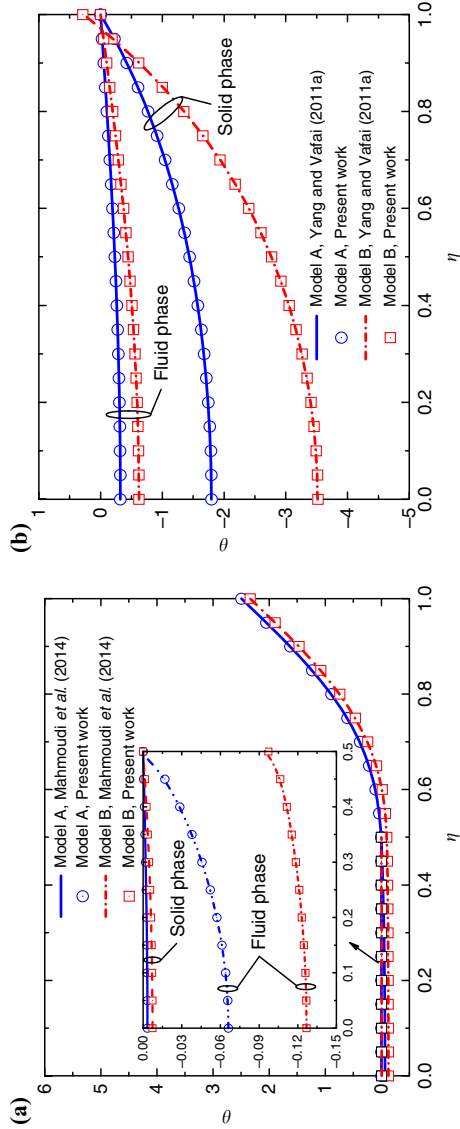
for Model A and:

$$\begin{aligned}
 \theta_{f,b}|_{Model\ B} = & \frac{A_3 C_4}{\omega^2 - \delta^2} [\omega \cosh(\delta \xi) \sinh(\omega \xi) - \delta \cosh(\omega \xi) \sinh(\delta \xi)] \\
 & + \frac{1}{4\kappa\omega} \frac{A_3^2(1+\gamma)}{\omega^2 - \delta^2} \left(1 - \frac{Bi}{\omega^2}\right) [2\omega \xi + \sinh(2\omega \xi)] \\
 & - \frac{A_3 P(1+\gamma)}{2(1+\kappa)} \frac{1}{\omega^3} [(2 + \omega^2 \xi^2) \sinh(\omega \xi) - 2\omega \xi \cosh(\omega \xi)] \\
 & + \frac{A_3}{\omega} \left[\frac{1}{1+\kappa} \left(\frac{P(1+\gamma)}{\kappa \delta^2} + C_3 \right) - \frac{P}{\kappa} \left(1 - \frac{Bi}{\omega^2}\right) \frac{1+\gamma}{\omega^2 - \delta^2} \right] \sinh(\omega \xi) \\
 & - C_4 \frac{P}{\delta} \sinh(\delta \xi) + \frac{P^2(1+\gamma)}{6(1+\kappa)} \xi^3 - \frac{P}{1+\kappa} \left(\frac{P(1+\gamma)}{\kappa \delta^2} + C_3 \right) \xi \\
 & + A_1 B_1 (1 - \xi) + \frac{1}{2} (A_1 B_2 + A_2 B_1) (1 - \xi^2) \\
 & + \frac{1}{6} \left[\frac{\varepsilon}{\kappa} (1 + \gamma) A_1^2 + 2A_2 B_2 + \frac{B_1 P}{Da} \right] (1 - \xi^3) \\
 & + \frac{1}{2} \left[\frac{\varepsilon}{3\kappa} A_1 A_2 (1 + \gamma) + \frac{B_2 P}{4Da} \right] (1 - \xi^4) \\
 & + \frac{1}{30} \frac{\varepsilon}{\kappa} \left(\frac{7P}{4Da} A_1 + A_2^2 \right) (1 + \gamma) (1 - \xi^5) \\
 & + \frac{1}{48} \frac{\varepsilon P}{\kappa Da} A_2 (1 + \gamma) (1 - \xi^6) + \frac{1}{336} \frac{\varepsilon}{\kappa} \left(\frac{P}{Da} \right)^2 (1 + \gamma) (1 - \xi^7) \quad (66)
 \end{aligned}$$

for Model B.

3. Results and discussion

To validate the present analytical solutions, we investigated both the partial and full filling cases in the absence of rarefaction effect (Yang and Vafai, 2011a; Mahmoudi *et al.*, 2014). In the validation, $\xi = 0.5$ is selected for the position of the porous-fluid interface for the partial filling case and $\xi = 1$ is done for the full filling one. As highlighted by some researchers (Bhargavi *et al.*, 2009; Satyamurty and Bhargavi, 2010), the optimal thermal performance for a partially filled system usually occurs at the porous substrate thickness fraction of 0.8 with the larger Darcy numbers (e.g. $Da = 10^{-3}$). Except Figure 2(b) for the validation and Figures 4(b) and 6(b) for regarding the effect of Darcy number on the studied thermal system, therefore, $Da = 10^{-3}$ is chosen in all the following calculations. Meanwhile, $\varepsilon = 0.9$ is considered for the porosity of porous medium throughout this study. It is worth noting that in the present work, the fluid and solid temperatures for both Models A and B are normalized with respect to the channel wall temperature T_w . However, the dimensionless temperatures for Models A and B obtained by Mahmoudi *et al.* (2014) and the ones for Model B derived by Yang and Vafai (2011a) are defined based on the solid phase temperature at the porous-fluid interface $T_{s,i}$. Thus, in the comparison all the results (except for Model A-based full filling case reported by Yang and Vafai, 2011a) using



Notes: (a) $\zeta=0.5, Da=10^{-3}$; (b) $\zeta=1, Da=10^{-5}$

Sources: Derived by (a) Mahmoudi *et al.* (2014), (b) Yang and Vafai (2011a)

Figure 2.
Comparison of the present analytical temperature distributions at $k=0.1, Bi=0.5, \epsilon=0.9$ and $Kn \rightarrow 0$

Equations (44), (46), (48), (56), (58) and (60) are modified utilizing the solid phase temperature at the interface as $\theta_{f1}-\theta_s(\xi)$, $\theta_{f2}-\theta_s(\xi)$ and $\theta_s-\theta_s(\xi)$. Additionally, the viscosity ratio $M=1$ is assumed for comparison with the results obtained by Mahmoudi *et al.* (2014). As stated by Mahmoudi *et al.* (2014), the case of $M=1$ leads to good results which agree fairly well with the experimental and numerical ones and so $M=1$ was utilized in the analysis. It should be noted that the effective viscosity of the fluid inside the porous medium strongly depends on the geometry of porous structure and the porosity. Due to very few works on the validity of $M=1$, numerous researchers have employed the relation $M = \mu_{eff}/\mu = \varepsilon^{-1}$ which is only a function of the porosity. As shown in Figure 2, the present analytical solutions of temperature distributions for Models A and B agree well with the available results in the literature (Yang and Vafai, 2011a; Mahmoudi *et al.*, 2014). It is noteworthy that the common continuum flow (no-slip flow), which corresponds to the limiting case of $Kn \rightarrow 0$, is only a special case of the slip flow.

Figure 3 depicts the effect of Knudsen number on the velocity distribution for different porous medium thicknesses $\xi = 0.2, 0.4, 0.6$ and 0.8 . As it is seen from all the subfigures, by increasing the porous substrate thickness more fluid particles escape to the clear region with less resistance, which leads to an increase in the maximum velocity. On the other hand, an increase in the Knudsen number leads to an increase in the velocity slip and consequently shifts the velocity peak toward the microchannel wall. As expected, this velocity peak is found to be located in the clear region. Additionally, in the porous region that is relatively far away from the interface, the velocity profile becomes flatter. At higher porous medium thickness, say $\xi = 0.8$, the narrow clear region causes an abrupt change in velocity in the vicinity of the interface.

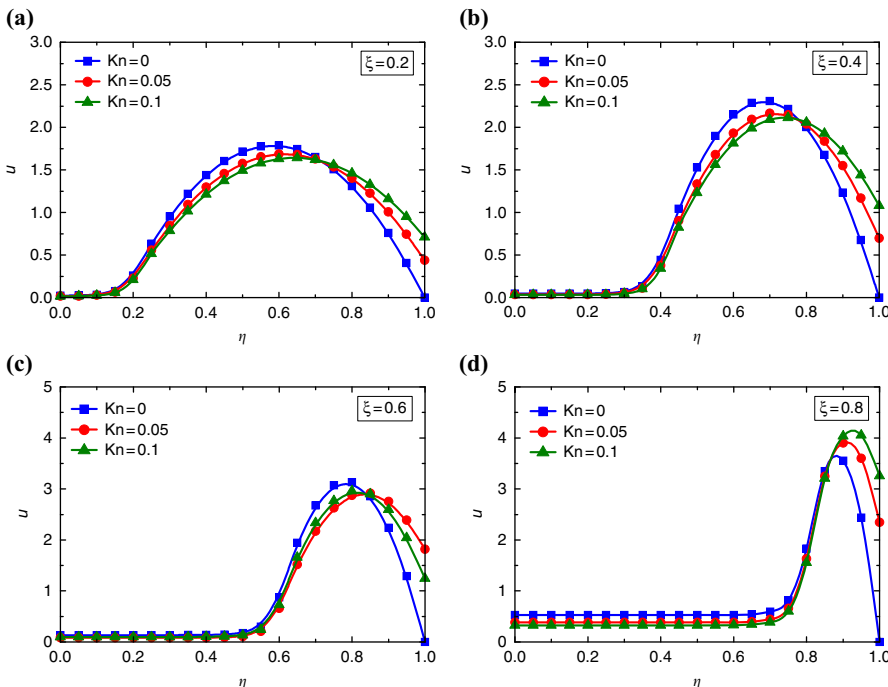


Figure 3.
Effect of the
Knudsen number on
the transverse
velocity distribution
at $Da = 10^{-3}$

The velocity gradients near both the wall and the interface for the slip flow regime decrease as compared to those obtained in the no-slip flow limit ($Kn \rightarrow 0$). This reveals that higher Kn reduces the retarding effect of the wall surface and yields more flow passing through the microchannel.

Figure 4 illustrates the effect of porous medium thickness on the heat flux distribution at the porous-fluid interface for Models A and B. As it is shown, an increase in the porous medium thickness leads to an enhancement in the amount of interfacial heat flux. For a given Da value (Figure 4(a)), the heat flux ratio γ decreases with increasing the Knudsen number while for a given Kn value (Figure 4(b)), the heat flux ratio increases with increasing the Darcy number. It is seen from both subfigures that the amount of interfacial heat flux transmitted from the clear fluid to the porous medium depends on the employed interface model, and interestingly, Model A predicts a higher heat flux ratio than Model B does. Similar trends with different Darcy numbers were also reported by Mahmoudi *et al.* (2014) without taking the rarefaction effect into account. With a reduction in Da , the difference between the amounts of heat flux at the interface predicted by Models A and B decreases. As expected, in the Darcy flow limit ($Da \rightarrow 0$), the amounts of heat flux predicted by both interface models will be equal.

Figure 5 delineates the dimensionless temperature distributions for the fluid and solid phases in the porous region with $Da = 10^{-3}$. It is seen that increasing Kn gives rise to an increase in the temperature jump at the wall. This is due to the reduction in the interaction between the gas molecules and the heated wall. For a given value of Kn , both models can predict substantial temperature difference between the fluid and solid phases within the porous region except Figure 5(c) and (d) with $\kappa = 0.01$ and $Bi = 10$. Higher Bi implies the strong internal heat exchange between the two phases within the porous region. As expected, this temperature difference would vanish when $Bi \rightarrow \infty$, which corresponds to the LTE case. Figure 5(a) and (e) clearly demonstrates that the less the effective thermal conductivity ratio the larger would be the chance to make marginal temperature difference. An interesting conclusion can be reached by comparing Figure 5(g) and (h). At larger effective thermal conductivity ratio, say $\kappa = 10$, the solid phase temperature in the porous region predicted by Model A is lower than the wall temperature whereas that predicted by Model B is higher than the wall temperature. This reveals that the partially porous system is sensitive to the interface models as the pertinent thermo-physical parameters vary. Therefore, choosing a more plausible interface model for splitting the heat flux between two individual phases within the porous substrate is heavily problem dependent (Mahmoudi and Maerefat, 2011; Yang and Vafai, 2011a, b, Vafai and Yang, 2013; Mahmoudi *et al.*, 2014).

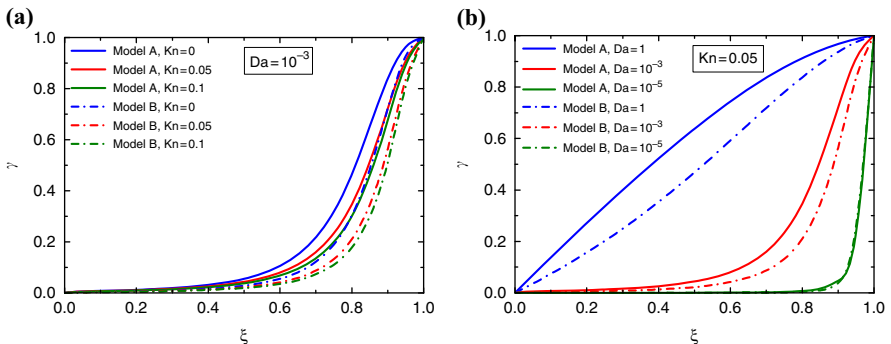


Figure 4.
Effect of the porous substrate thickness on the interface heat flux distribution

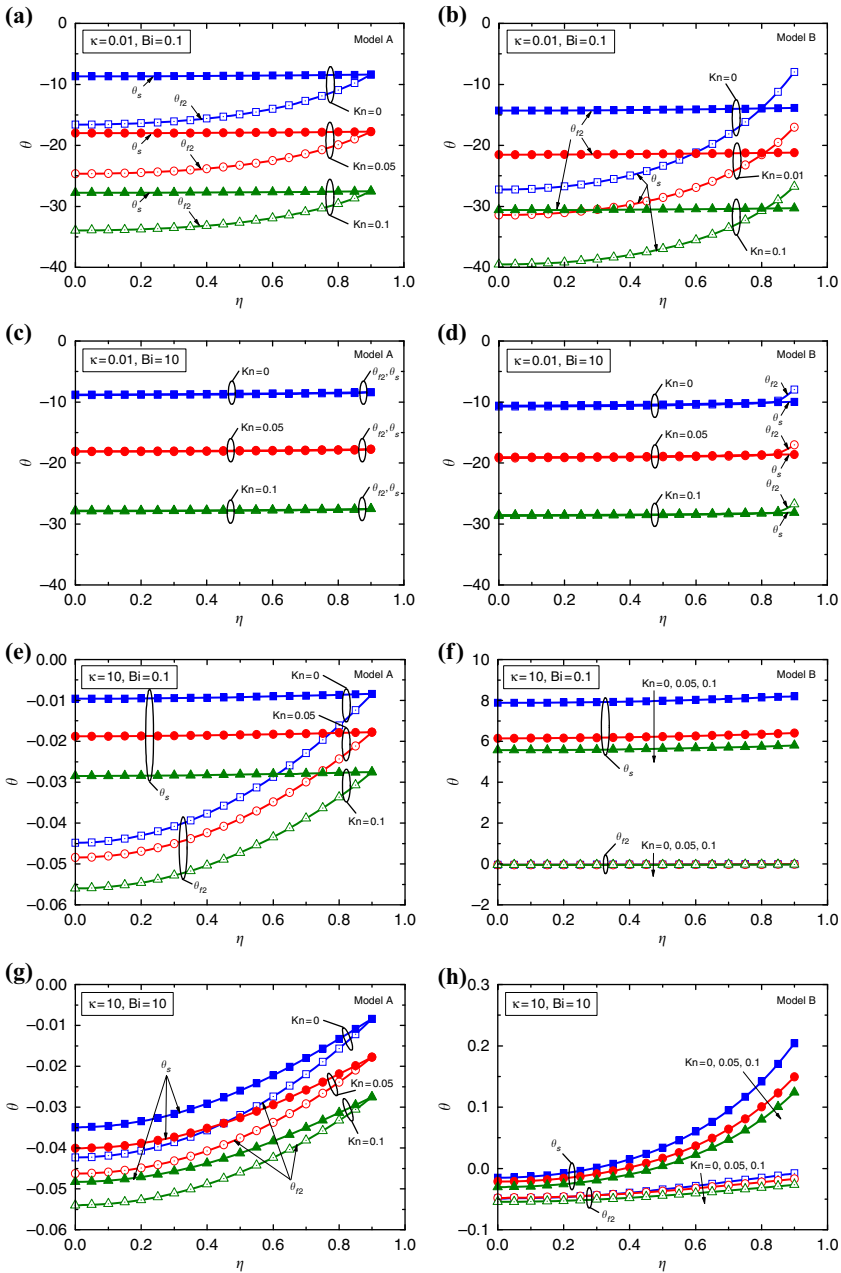
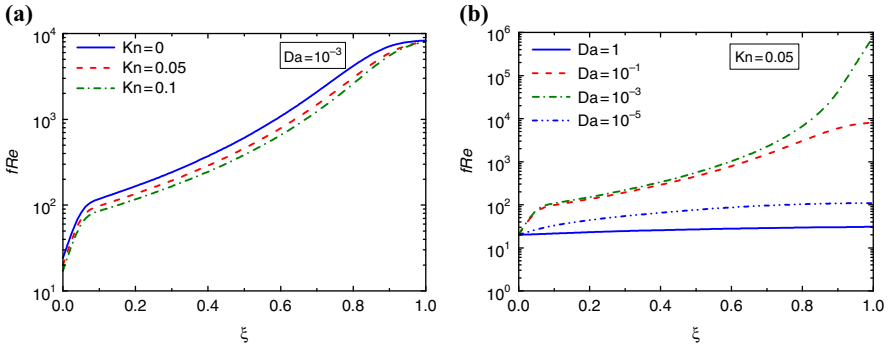


Figure 5.
Effect of the
Knudsen number on
the temperature
distribution in the
porous region at
 $Da = 10^{-3}$

Figure 6 shows the variation of pressure drop fRe with the porous thickness together with the Darcy and Knudsen numbers. For a given Darcy number, say $Da = 10^{-3}$ as shown in Figure 6(a), the pressure drop decreases as the Knudsen number increases. As is well known, an increase in the Knudsen number would result in an enhancement in Re due to

Figure 6.
Effect of the porous substrate thickness on the pressure drop



Notes: (a) Different Knudsen numbers at $Da = 10^{-3}$; (b) different Darcy numbers at $Kn = 0.05$

an increase in the flow velocity and a reduction in f due to the velocity slip at the walls. However, the Fanning friction factor predominates in the competition with the Reynolds number and thereby leads to the reduction in fRe . For a given Knudsen number, say $Kn = 0.05$ as shown in Figure 6(b), the pressure drop is increased by increasing the porous thickness for different values of the Darcy number. At larger values of $Da \geq 1$, fRe is almost independent of ξ due to the similar influences of f and Re on their product.

Figure 7 shows the variation of Nusselt number predicted by Models A and B with the porous substrate thickness. As it is well known and expected, for a given

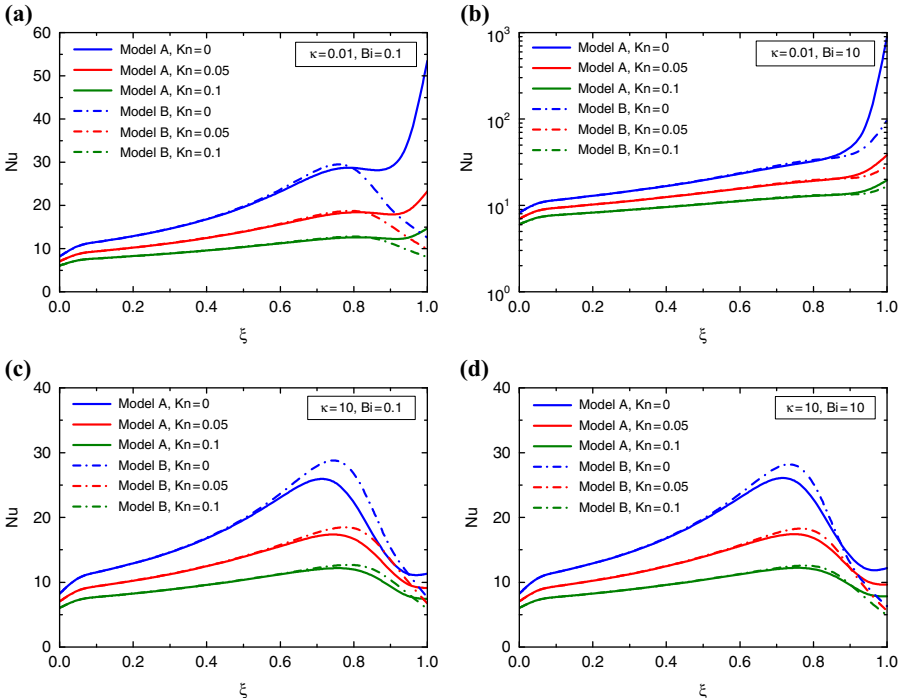


Figure 7.
Effect of the porous substrate thickness on the Nusselt number for different Knudsen numbers

value of ξ , an increase in the Knudsen number causes a reduction in the Nusselt number due to rarefaction. For all considered combinations of κ and Bi , Figure 7(a), (c) and (d) illustrates that there exists a critical porous thickness ξ_{cr} below which the Nusselt numbers monotonically increase for both Models A and B while above which the values of Nu decrease monotonically except those obtained for Model A as shown in Figure 7(a). The Nusselt number for Model A $\kappa = 0.01$ and $Bi = 0.1$ exhibits a complicated increase-decrease-increase behavior. As for Figure 7(b) with $\kappa = 0.01$ and $Bi = 10$, a monotonical increase in the Nusselt number occurs for both interface models from the clear fluid limit ($\xi \rightarrow 0$) to the full filling limit ($\xi \rightarrow 1$). Table I compares the critical values of porous substrate thickness for both interface models. The tabulated results clearly illustrate that the maximum enhancement in heat transfer occurs around at a porous fraction of 0.8 for Darcy number of 10^{-3} . This coincides the findings reported for the partially porous systems excluding the rarefaction effect (Mohamad, 2003; Yang and Hwang, 2009; Satyamurty and Bhargavi, 2010; Mahmoudi and Maerefat, 2011; Nimvari *et al.*, 2012; Mahmoudi *et al.*, 2014). By comparing Figure 7(c) and (d), at higher κ the Nusselt number for $Bi = 0.1$ shows a similar behavior with that for $Bi = 10$.

Although the porous media are helpful for heat transfer enhancement, their insertion will impose large pressure drop within a composite thermal system. Therefore, it is important to seek a compromise between the heat transfer and the pressure drop in evaluating the thermal performance. Herein, a parameter which serves as a thermal hydrodynamic measure of the heat transfer efficiency such that $\Phi = (Nu)_p(fRe)_o / [(Nu)_o(fRe)_p]$ (Cekmer *et al.*, 2012; Mahmoudi *et al.*, 2014) in which the subscripts p and o denote the values for a microchannel with or without a porous insert, respectively. Figure 8 depicts the variation of the heat transfer efficiency for both Models A and B with the porous substrate thickness. In all subfigures, the value of $\Phi = 1$ represents the heat transfer efficiency for the clear fluid limit ($\xi \rightarrow 0$). It is apparent that for lower κ , say $\kappa = 0.01$ as shown in Figure 8(a) and (b), the heat transfer efficiency is not remarkably impacted by the Knudsen number only when $\xi < 0.8$. However, for a fixed value of Bi , the dependence of Φ on the Knudsen number is not significant over the entire range of ξ by increasing κ from 0.01 to 10. As illustrated in Figures 6 and 7, the pressure drop obtained at around $\xi = 0.8$ is relatively not serious while the corresponding Nusselt number is much higher than that of the clear microchannel. Hence, the threshold value of 0.8 may be considered as an optimal filling thickness ξ_{opt} for enhancing heat transfer in the partially porous microchannels at a reasonable expense of pressure drop.

Subfigure	Interface model	$Kn = 0$	$Kn = 0.05$	$Kn = 0.1$
Figure 7(a)	A	–	–	–
	B	0.75	0.80	0.80
Figure 7(b)	A	–	–	–
	B	–	–	–
Figure 7(c)	A	0.70	0.75	0.75
	B	0.80	0.75	0.80
Figure 7(d)	A	0.70	0.75	0.75
	B	0.75	0.75	0.80

Table I.
Comparison of the
critical porous
thickness for Models
A and B at
 $Da = 10^{-3}$

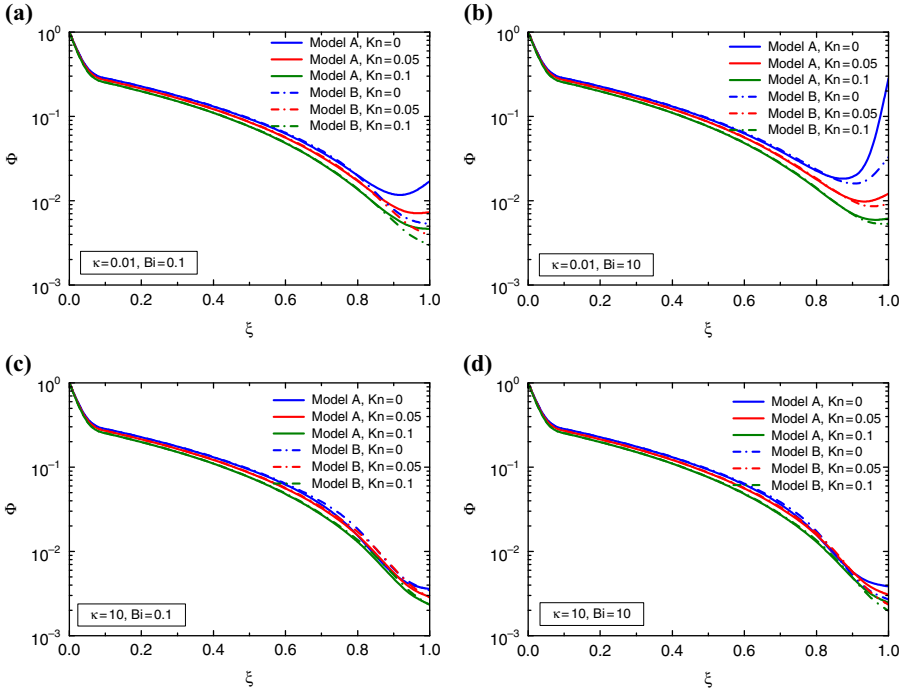


Figure 8.
Effect of the porous substrate thickness on the heat transfer efficiency for different Knudsen numbers

4. Conclusions

Gaseous slip flow and heat transfer analysis is analytically performed within a parallel-plate microchannel partially filled with a centered porous medium under LTNE condition. Both Models A and B are utilized to consider the heat flux splitting for the fluid and solid phases at the porous-fluid interface. Analytical solutions for the fluid and solid phase temperature distributions and the Nusselt number are derived. In the no-slip flow limit ($Kn \rightarrow 0$), the present analytical solutions are validated by the partially and fully filled cases available in the literature. In other words, the continuum flow (no-slip flow) is only a special case of the slip counterpart. Meanwhile, the effects of pertinent parameters such as κ , Bi , Kn , Da and ξ on the heat transfer are also discussed. An increase in the Knudsen number leads to an increase in the velocity slip and consequently shifts the velocity peak toward the microchannel wall. Higher Kn reduces the retarding effect of the wall surface and yields more flow passing through the microchannel. The difference between the amounts of heat flux at the interface predicted by Models A and B decreases by reducing the Darcy number. As expected, when Da approaches zero, the amounts of heat flux predicted by both models will be equal. At larger effective thermal conductivity ratio, say $\kappa = 10$, the solid phase temperature in the porous region predicted by Model A is lower than the wall temperature whereas that predicted by Model B exhibits an opposite trend. Compared with the results obtained for the continuum flow regime, the gas rarefaction negatively impacts the heat transfer efficiency and has little influence on the optimal porous thickness of 0.8. Actually, this work is an extension of our previous studies on the fully filled porous structures (Wang *et al.*, 2015b, c).

References

- Amiri, A., Vafai, K. and Kuzay, T.M. (1995), "Effect of boundary conditions on non-Darcian heat transfer through porous media and experimental comparisons", *Numerical Heat Transfer, Part A*, Vol. 27 No. 6, pp. 651-664.
- Bahrami, H., Bergman, T.L. and Faghri, A. (2012), "Forced convective heat transfer in a microtube including rarefaction, viscous dissipation and axial conduction effects", *International Journal of Heat and Mass Transfer*, Vol. 55 No. 23, pp. 6665-6675.
- Bhargavi, D., Satyamurty, V.V. and Raja Sekhar, G.P. (2009), "Effect of porous fraction and interfacial stress jump on skin friction and heat transfer in flow through a channel partially filled with porous material", *Journal of Porous Media*, Vol. 12 No. 11, pp. 1065-1082.
- Buonomo, B., Manca, O. and Lauriat, G. (2014), "Forced convection in micro-channels filled with porous media in local thermal non-equilibrium conditions", *International Journal of Thermal Science*, Vol. 77 No. 1, pp. 206-222.
- Cai, C., Sun, Q. and Boyd, I.D. (2007), "Gas flows in microchannels and microtubes", *Journal of Fluid Mechanics*, Vol. 589 No. 6, pp. 305-314.
- Cekmer, O., Mobedi, M., Ozerdem, B. and Pop, I. (2012), "Fully developed forced convection in a parallel plate channel with a centered porous layer", *Transport in Porous Media*, Vol. 93 No. 1, pp. 179-201.
- Chen, X., Tavakkoli, F. and Vafai, K. (2015), "Analysis and characterization of metal foam filled double-pipe heat exchangers", *Journal of Numerical Heat Transfer*, Vol. 68 No. 10, pp. 1031-1049.
- de Souza Mendes, P.R. (2007), "Dimensionless non-Newtonian fluid mechanics", *Journal of Non-Newtonian Fluid Mechanics*, Vol. 147 No. 1, pp. 109-116.
- Glicksman, L.R. (1988), "Scaling relationships for fluidized beds", *Chemical Engineering Science*, Vol. 43 No. 6, pp. 1419-1421.
- Haddad, O.M., Al-Nimr, M.A. and Sari, M.S. (2007), "Forced convection gaseous slip flow in circular porous micro-channels", *Transport in Porous Media*, Vol. 70 No. 2, pp. 167-179.
- Hooman, K. (2009), "Slip flow forced convection in a microporous duct of rectangular cross-section", *Applied Thermal Engineering*, Vol. 29 No. 5, pp. 1012-1019.
- Karniadakis, G., Beskok, A. and Aluru, N. (2005), *Micro Flows and Nano Flows: Fundamentals and Simulation*, Springer, New York, NY.
- Lasiello, M., Vafai, K., Andreozzi, A., Bianco, N. and Tavakkoli, F. (2015), "Effects of external and internal hyperthermia on LDL transport and accumulation within an arterial wall in the presence of stenosis", *Annals of Biomedical Engineering*, Vol. 43 No. 7, pp. 1585-1599.
- Lee, D.Y. and Vafai, K. (1999), "Analytical characterization and conceptual assessment of solid and fluid temperature differentials in porous media", *International Journal of Heat and Mass Transfer*, Vol. 42 No. 3, pp. 423-435.
- Mahdavi, M., Saffar-Avval, M., Tiari, S. and Mansoori, Z. (2014), "Entropy generation and heat transfer numerical analysis in pipes partially filled with porous medium", *International Journal of Heat and Mass Transfer*, Vol. 79, pp. 496-506.
- Mahjoob, S. and Vafai, K. (2009a), "Analytical characterization of heat transfer through biological media incorporating hyperthermia treatment", *International Journal of Heat and Mass Transfer*, Vol. 52 No. 5, pp. 1608-1618.
- Mahjoob, S. and Vafai, K. (2009b), "Analytical characterization and production of an isothermal surface for biological and electronic applications", *ASME Journal of Heat Transfer*, Vol. 131 No. 5, pp. 052604.1-052604.12.
- Mahmoudi, Y. (2015), "Constant wall heat flux boundary condition in micro-channels filled with a porous medium with internal heat generation under local thermal non-equilibrium condition", *International Journal of Heat and Mass Transfer*, Vol. 85, pp. 524-542.

- Mahmoudi, Y. and Maerefat, M. (2011), "Analytical investigation of heat transfer enhancement in a channel partially filled with a porous material under local thermal non-equilibrium condition", *International Journal of Thermal and Sciences*, Vol. 50 No. 12, pp. 2386-2401.
- Mahmoudi, Y., Karimi, N. and Mazaheri, K. (2014), "Analytical investigation of heat transfer enhancement in a channel partially filled with a porous material under local thermal non-equilibrium condition: effects of different thermal boundary conditions at the porous-fluid interface", *International Journal of Heat and Mass Transfer*, Vol. 70, pp. 875-891.
- Mohamad, A.A. (2003), "Heat transfer enhancements in heat exchangers fitted with porous media part I: constant wall temperature", *International Journal of Thermal and Sciences*, Vol. 42 No. 4, pp. 385-395.
- Narasimhan, A., Lage, J. and Nield, D.A. (2001), "New theory for forced convection through porous media by fluids with temperature-dependent viscosity", *ASME Journal of Heat Transfer*, Vol. 123 No. 6, pp. 1045-1051.
- Nield, D.A. and Kuznetsov, A.V. (2007), "Reply to comments on 'forced convection with slip-flow in a channel or duct occupied by a hyper-porous medium saturated by a rarefied gas'", *Transport in Porous Media*, Vol. 67 No. 1, pp. 169-170.
- Nimvari, M.E., Maerefat, M. and El-Hossaini, M.K. (2012), "Numerical simulation of turbulent flow and heat transfer in a channel partially filled with a porous media", *International Journal of Thermal and Sciences*, Vol. 60 No. 1, pp. 131-141.
- Pavel, B.I. and Mohamad, A.A. (2004), "An experimental and numerical study on heat transfer enhancement for gas heat exchangers fitted with porous media", *International Journal of Heat and Mass Transfer*, Vol. 47 No. 23, pp. 4939-4952.
- Qu, Z.G., Xu, H.J. and Tao, W.Q. (2012), "Fully developed forced convective heat transfer in an annulus partially filled with metallic foams: an analytical solution", *International Journal of Heat and Mass Transfer*, Vol. 55 No. 25, pp. 7508-7519.
- Renksizbulut, M., Niazmand, H. and Tercan, G. (2006), "Slip-flow and heat transfer in rectangular microchannels with constant wall temperature", *International Journal of Thermal and Sciences*, Vol. 45 No. 9, pp. 870-881.
- Satyamurty, V.V. and Bhargavi, D. (2010), "Forced convection in thermally developing region of a channel partially filled with a porous material and optimal porous fraction", *International Journal of Thermal and Sciences*, Vol. 49 No. 2, pp. 319-332.
- Shokouhmand, H., Jam, F. and Salimpour, M.R. (2011), "The effect of porous insert position on the enhanced heat transfer in partially filled channels", *International Communications in Heat and Mass Transfer*, Vol. 38 No. 8, pp. 1162-1167.
- Torabi, M., Zhang, K.L., Yang, G.C., Wang, J. and Wu, P. (2015), "Heat transfer and entropy generation analyses in a channel partially filled with porous media using local thermal non-equilibrium model", *Energy*, Vol. 82 No. 67, pp. 922-938.
- Vafai, K. and Kim, S.J. (1990), "Fluid mechanics of the interface region between a porous medium and a fluid layer – an exact solution", *International Journal of Heat and Fluid Flow*, Vol. 11 No. 3, pp. 254-256.
- Vafai, K. and Yang, K. (2013), "A note on local thermal non-equilibrium in porous media and heat flux bifurcation phenomenon in porous media", *Journal of Transport in Porous Media*, Vol. 96 No. 1, pp. 169-172.
- Wang, K.Y., Tavakkoli, F. and Vafai, K. (2015a), "Analysis of gaseous slip flow in a porous micro-annulus under local thermal non-equilibrium condition – an exact solution", *International Journal of Heat and Mass Transfer*, Vol. 89, pp. 1331-1341.
- Wang, K.Y., Wang, D.Z. and Li, P.C. (2015b), "Two decoupling methods for the heat transfer model of a plate channel filled with a porous medium", *Journal of Applied Mathematics*, Vol. 36 No. 5, pp. 494-504 (in Chinese).

Wang, K.Y., Tavakkoli, F., Wang, S.J. and Vafai, K. (2015c), "Analysis and analytical characterization of bio heat transfer during radiofrequency ablation", *Journal of Biomechanics*, Vol. 48 No. 6, pp. 930-940.

Wang, K.Y., Tavakkoli, F., Wang, S.J. and Vafai, K. (2015d), "Forced convection gaseous slip flow in a porous circular microtube: an exact solution", *International Journal of Thermal and Sciences*, Vol. 97, pp. 152-162.

Xu, H.J., Qu, Z.G. and Tao, W.Q. (2011), "Analytical solution of forced convective heat transfer in tubes partially filled with metallic foam using the two-equation model", *International Journal of Heat and Mass Transfer*, Vol. 54 No. 17, pp. 3846-3855.

Yang, C., Nakayama, A. and Liu, W. (2012), "Heat transfer performance assessment for forced convection in a tube partially filled with a porous medium", *International Journal of Thermal and Sciences*, Vol. 54 No. 1, pp. 98-108.

Yang, K. and Vafai, K. (2010), "Analysis of temperature gradient bifurcation in porous media – an exact solution", *International Journal of Heat and Mass Transfer*, Vol. 53 No. 19, pp. 4316-4325.

Yang, K. and Vafai, K. (2011a), "Analysis of heat flux bifurcation inside porous media incorporating inertial and dispersion effects – an exact solution", *International Journal of Heat and Mass Transfer*, Vol. 54 No. 25, pp. 5286-5297.

Yang, K. and Vafai, K. (2011b), "Restrictions on the validity of the thermal conditions at the porous-fluid interface – an exact solution", *ASME Journal of Heat Transfer*, Vol. 133 No. 11, pp. 112601.1-112601.12.

Yang, Y.T. and Hwang, M.L. (2009), "Numerical simulation of turbulent fluid flow and heat transfer characteristics in heat exchangers fitted with porous media", *International Journal of Heat and Mass Transfer*, Vol. 52 No. 13, pp. 2956-2965.

Yuan, X., Tavakkoli, F. and Vafai, K. (2015), "Analysis of natural convection in a horizontal concentric annuli with different inner shapes", *Journal of Numerical Heat Transfer*, Vol. 68 No. 11, pp. 1155-1174.

Zehforoosh, A. and Hossainpour, S. (2010), "Numerical investigation of pressure drop reduction without surrendering heat transfer enhancement in partially porous channel", *International Journal of Thermal and Sciences*, Vol. 49 No. 9, pp. 1649-1662.

Appendix

The constants A_1 , A_2 and A_3 involved in Equations (32) and (33) are given by:

$$A_1 = \frac{\Phi_1}{\Phi_4}P, \quad A_2 = \frac{\Phi_2}{\Phi_4}P, \quad A_3 = \frac{\Phi_3}{\Phi_4}P \tag{A1}$$

where:

$$\Phi_1 = [2\xi(1 + \alpha) - 2\alpha - 1]\cosh(\omega \xi) - M \{ \xi[\xi(1 + \alpha) - 2\alpha - 1] + 2(1 + \alpha)Da \} \omega \sinh(\omega \xi) \tag{A2}$$

$$\Phi_2 = -2\xi \cosh(\omega \xi) + M(\xi^2 + 2Da - 2\alpha - 1)\omega \sinh(\omega \xi) \tag{A3}$$

$$\Phi_3 = (1 - \xi)(\xi - 2\alpha - 1) + 2Da \tag{A4}$$

$$\Phi_4 = 2[\cosh(\omega \xi) + M(1 - \xi + \alpha)\omega \sinh(\omega \xi)]Da \tag{A5}$$

The following compatibility:

$$\int_0^{\xi^-} \hat{u}_{f2} d\eta + \int_{\xi^+}^1 \hat{u}_{f1} d\eta = 1 \tag{A6}$$

which is obtained by substituting Equation (25) into Equation (17) must be satisfied identically. Thus, substituting Equations (32) and (33) into Equation (A6) leads to the dimensionless pressure gradient:

$$P = \left\{ \frac{1}{\Phi_4} \left[\Phi_1(1 - \xi) + \frac{\Phi_2}{2}(1 - \xi^2) + \frac{\Phi_3}{\omega} \sinh(\omega \xi) \right] + \frac{1 - \xi^3}{6Da - \xi} \right\}^{-1} \tag{A7}$$

The constants B_1, B_2, B_3 and B_4 involved in Equations (44), (46) and (48) can be determined by applying the boundary conditions given by Equations (42) and (43) as:

$$B_1 = -\frac{\varepsilon}{6\kappa} \left[\beta \left(6A_1 + 3A_2 + \frac{P}{\text{Da}} \right) + 3A_1 + A_2 + \frac{P}{4\text{Da}} \right] - (1 + \beta)B_2 \quad (\text{A8})$$

$$B_2 = \frac{\varepsilon}{\kappa} \left[1 - \frac{1}{6} \left(6A_1 + 3A_2 + \frac{P}{\text{Da}} \right) \right] \quad (\text{A9})$$

$$B_3 = (1 + \kappa) \left[B_1 + B_2 \zeta + \frac{\varepsilon}{6\kappa} \left(3A_1 \zeta^2 + A_2 \zeta^3 + \frac{P}{4\text{Da}} \zeta^4 \right) - B_4 \cosh(\delta \zeta) - \frac{A_3}{\kappa} \left(1 - \frac{\text{Bi}}{\omega^2} \right) \frac{\cosh(\omega \zeta)}{\omega^2 - \delta^2} + \frac{P}{1 + \kappa} \left(\frac{\zeta^2}{2} - \frac{1}{\kappa \delta^2} \right) \right] \quad (\text{A10})$$

$$B_4 = -\frac{1}{\kappa(1 + \kappa) \cosh(\delta \zeta)} \left[\frac{A_3 \cosh(\omega \zeta)}{\omega^2 - \delta^2} + \frac{P}{\delta^2} \right] \quad (\text{A11})$$

The constant B'_3 involved in Equation (49) is given by:

$$B'_3 = (1 + \kappa) \left[B_1 + B_2 \zeta + \frac{\varepsilon}{6\kappa} \left(3A_1 \zeta^2 + A_2 \zeta^3 + \frac{P}{4\text{Da}} \zeta^4 \right) \right] - \frac{A_3}{\omega^2} \cosh(\omega \zeta) - \frac{P}{2\zeta^2} \quad (\text{A12})$$

The constants C_1, C_2, C_3 and C_4 involved in Equations (56), (58) and (60) can be determined by applying the boundary conditions given by Equations (54) and (55) as:

$$C_1 = -\frac{\varepsilon(1 + \gamma)}{6\kappa} \left[\beta \left(6A_1 + 3A_2 + \frac{P}{\text{Da}} \right) + 3A_1 + A_2 + \frac{P}{4\text{Da}} \right] - (1 + \beta)C_2 \quad (\text{A13})$$

$$C_2 = \frac{\varepsilon}{\kappa} \left[1 - \frac{1 + \gamma}{6} \left(6A_1 + 3A_2 + \frac{P}{\text{Da}} \right) \right] \quad (\text{A14})$$

$$C_3 = (1 + \kappa) \left[C_1 + C_2 \zeta + \frac{\varepsilon(1 + \gamma)}{6\kappa} \left(3A_1 \zeta^2 + A_2 \zeta^3 + \frac{P}{4\text{Da}} \zeta^4 \right) - C_4 \cosh(\delta \zeta) - \frac{A_3}{\kappa} (1 + \gamma) \left(1 - \frac{\text{Bi}}{\omega^2} \right) \frac{\cosh(\omega \zeta)}{\omega^2 - \delta^2} + \frac{1 + \gamma}{1 + \kappa} \left(\frac{\zeta^2}{2} - \frac{1}{\kappa \delta^2} \right) P \right] \quad (\text{A15})$$

$$C_4 = \frac{1}{\delta \sinh(\delta \zeta)} \left[\frac{\gamma}{\kappa} - \frac{A_3}{\kappa} (1 + \gamma) \left(1 - \frac{\text{Bi}}{\omega^2} \right) \frac{\omega \sinh(\omega \zeta)}{\omega^2 - \delta^2} + \frac{1 + \gamma}{1 + \kappa} P \zeta \right] \quad (\text{A16})$$

Corresponding author

Kambiz Vafai can be contacted at: vafai@engr.ucr.edu

For instructions on how to order reprints of this article, please visit our website:

www.emeraldgroupublishing.com/licensing/reprints.htm

Or contact us for further details: permissions@emeraldinsight.com